RESEARCH ARTICLE

Effect of High-voltage Electrostatic Field on Potassium and Phosphate Uptake by Cucumber Plants

Jianyun Zhu[1,2] **and Meiqing Li**[1,2,*]

[1] Key Laboratory of Modern Agricultural Equipment and Technology, Ministry of Education, China
[2] College of Agricultural Engineering, Jiangsu University, Zhenjiang 212013, China

Abstract

An individual plant cell functions as a complex dynamic circuit, composed of resistor, capacitor, and inductor networks created by cellular structures and macromolecules. Furthermore, high-voltage electrostatic fields (HVEF) alter its electrical properties and initiate metabolic changes. This study aimed to examine the impact of HVEF on the kinetic properties of potassium (K^+) and phosphate ($H_2PO_4^-$) absorption by *Cucumis sativus* L. seedlings, and further probed the regulatory mechanisms by constructing a cell membrane potential model. Experimental findings revealed that HVEF substantially altered the maximum uptake rate (I_{max}), half-saturation constant (K_m), and minimum critical concentration (C_{min}) of K^+ and $H_2PO_4^-$ absorption in cucumber seedlings. Additionally, the regulatory effects displayed a clear dependence on the intensity of the HVEF. Potassium uptake increased as the intensity rose to 1 kV/cm, before declining between 1 and 2 kV/cm. Likewise, phosphate uptake increased as the intensity reached 0.5 kV/cm, before decreasing between 0.5 and 2 kV/cm. A spherical cell model, based on Poisson's equation, indicated that HVEF caused asymmetric membrane potential shifts (hyperpolarization on the lower hemisphere and depolarization on the upper hemisphere), controlling the opening and closing of ion channels. This research offers a theoretical foundation for the use of HVEF in modulating plant nutrient uptake.

Keywords: Cucumis sativus L., depolarization, high-voltage electric field, hyperpolarization, ion absorption kinetics.

1 Introduction

A single plant cell acts as a sophisticated dynamic circuit, composed of resistor, capacitor and inductor networks from cellular structures and macromolecules that encode physiological states via interactions. Metabolic and biochemical processes reflect changes in these electrical component networks, with their energy storage and conversion manifesting as cellular metabolism [1]. High-voltage electrostatic fields (HVEF), as an energy form, inevitably alter plant cellular electrical behavior and induce metabolic changes when applied to plants.

The biological effects of HVEFs on plants have been investigated over the last few decades. In addition to increasing dry weight [2], plant heights, and leaf surface areas [3], HVEFs have been shown to improve germination [4, 5], affect photosynthesis

Submitted: 01 November 2025
Accepted: 23 February 2026
Published: 11 March 2026

Vol. 1, **No.** 1, 2026.
10.62762/JPE.2025.597638

***Corresponding author:**
Meiqing Li
lmqljy@163.com

Citation
Zhu, J., & Li, M. (2026). Effect of High-voltage Electrostatic Field on Potassium and Phosphate Uptake by Cucumber Plants. *Journal of Plant Electrobiology*, 1(1), 32–41.

© 2026 ICCK (Institute of Central Computation and Knowledge)

and respiration rates [6], and alter hydrogen and carbon dioxide output rates. Moreover, the application of electric fields can influence nutrient uptake. It has been proven that HVEFs may accelerate the cotransport of several ion species, such as nitrogen [7, 8], potassium [9], and phosphate [10], and increase the amount and activity of plasma membrane enzymes involved in channels for ion absorption.

The application of electric fields can alter membrane potential, which plays a crucial role in nutrient uptake [11]. Some external stresses, such as salt stress, can also disrupt membrane potential [12]. The membrane potential, caused by charge separation, can change the permeability of the plasma membrane and control the transport of nutrients across the cell membrane [10, 13, 14]. Conversely, ion uptake can also alter the membrane potential [15–18]. Therefore, it is speculated that the effects of HVEFs on ion uptake may be related to the alteration of membrane potential induced by these fields.

Soil phosphorus cycling and efficient phosphorus utilization represent core issues in agricultural nutrient management. It has been established that land-use changes and agricultural practices exert a profound regulatory influence on the entire process of soil phosphorus cycling and crop phosphorus absorption [19]. Optimized phosphorus application measures can not only enhance soil enzymatic activity but also effectively improve crop nutritional status and promote biomass accumulation by augmenting phosphorus incorporation efficiency [20]. This underscores the significance of exploring artificial regulation strategies for crop nutrient uptake to enhance fertilizer use efficiency. Moreover, ion homeostasis serves as the foundation for maintaining normal plant physiological metabolism, particularly under abiotic stress such as salinity. Ammonium nitrate can mitigate the damage caused by salt stress to *Vigna radiata* L. by regulating plant physiological characteristics and phytohormone metabolism to uphold ion balance [21]. *Pseudomonas putida* RT12 is also capable of enhancing the salinity tolerance of peas through the mediation of ion homeostasis, osmotic adjustment, and reactive oxygen species detoxification [22]. As a physical regulatory approach, HVEF has been proven to exert an influence on crop ion absorption. Its regulatory effect on ion homeostasis is expected to provide a novel technical approach for enhancing crop nutrient utilization efficiency and stress resistance.

The Michaelis-Menten kinetic equation, which describes the kinetics of ion absorption, has been employed extensively to convey the information about ion uptake by plants [23, 24]. Extracellular electric-field-induced membrane potential changes are well described by Poisson's equation of electrostatics [11]. However, while some research has demonstrated the effect of HVEF on ion absorption, little information has been provided on the kinetics of HVEF-induced nutrient uptake, particularly in the simultaneous case of potassium and phosphate.. Besides, the effects of these fields on membrane potential have not been examined to date. Therefore, this study investigated the kinetic effect of HVEFs on potassium and phosphate absorption by plants. Poisson's equation was employed to a cell model on membrane potential that attempted to explain the kinetics changes caused by HVEF.

2 Material and Methods

2.1 Cucumber plant seedling preparation

Cultivated all over the world, *Cucumis sativus* L. has been known for its great demand for potassium and phosphate. Hence, *C. sativus* L. was chosen as experimental material in this work. Cucumber (*C. sativus* L.) seeds were surface sterilized with 0.5% (w/v) aqueous formalin for 30 min, washed, and imbibed with distilled water for 24 h. After germination, the seedlings were transferred into quartz sand under a 16 h/8 h light/dark cycle at 25 $\pm$ 1 °C and an irradiance of 600 μmol/m^2 s and cultured with a regular supply of fresh Hoagland nutrient solution for 30 days. Next, they were irrigated with 1 mM $CaSO_4$ starvation solutions for 2 days and used for cell absorption experiments.

2.2 Reagents and solutions

Nutrient solutions were prepared from analytical grade potassium nitrate and ammonium dihydrogen phosphate. Double-distilled water was used throughout the analyses. Potassium or phosphate concentrations amounted to 1 mmol/L.

2.3 HVEF treatment system

2.3.1 Experimental setup

HVEF treatments were performed using a laboratory-scale high electric field apparatus with a maximum output of 100 kV. As shown in Figure 1, this apparatus included a BGG100KV/2MA power generator (Beijing Electrical and Mechanical Institute, Beijing, China), two rectangular 40 cm×60

cm stainless steel plates used as electrodes, a high-voltage controller, a voltmeter, an ammeter , and an electrostatic shield.

2.3.2 Generation of electrostatic field

The generator created an electric charge that produced a high voltage between the stainless steel electrodes (Figure 1). The adjustable cathode–anode distance provided different electric field strengths. A parallel plate setup resulted in quasi-uniform interelectrode fields and the electric field strength was estimated according to the following equation:

$$\text{Electric field strength (kV/cm)} = \frac{\text{Voltage (kV)}}{\text{Distance (cm)}} \tag{1}$$

In this study, the output voltage was variable for an interelectrode distance of 20 cm [15].

2.4 Absorption experiment

Ten starved seedlings were placed in 100 mL beakers in the presence of the corresponding nutrient solution (80 mL) and exposed to electric field intensities of 0.5, 1.0, 1.5, 2.0, 2.5, and 3.0 kV/cm. The entire experiment proceeded in an artificial climate chamber at 25 $\pm$1 °C with a relative humidity of 60%–70% and a photon flux density of 200 μmol/m^{2}s. The pH in absorption solution was 7.5 for KNO_3 and 7.7 for $NH_4H_2PO_4$, respectively.

Control seedlings were placed between the same electrode plates with the voltage switched off, so that temperature, airflow, humidity, electrostatic shielding and mechanical support conditions were identical between control and HVEF treatments.

For each HVEF treatment, five independent beakers were used, each containing ten starved seedlings (biological replicates). Ion uptake at a given HVEF level was calculated as the means of these five independent experimental units. The first sampling at 10 min was chosen to capture the initial, approximately linear uptake phase, while subsequent samplings at 60 min intervals allowed us to follow the depletion of nutrients over a sufficiently long period (7 h) without excessively disturbing the system. This sampling scheme provided enough data points to fit the depletion curves and extract kinetic parameters while keeping the experimental procedure practical.

The 7-h uptake period was selected to obtain sufficient depletion data for reliable kinetic fitting. To maintain transporter activity and membrane integrity during this period, all experiments were conducted under controlled temperature, humidity and light conditions in an artificial climate chamber, and the seedlings had been pre-starved in $CaSO_4$ solution for 2 days to minimize metabolic shifts during the measurement. In addition, the nutrient solutions were not renewed during the 7-h uptake period, so the observed depletion curves reflect a continuous uptake process rather than repeated perturbations.

Because a solution-depletion technique was employed, each uptake experiment consisted of a full-time course of nutrient depletion rather than a single end-point measurement. Kinetic parameters (I_{max}, K_m and C_{min}) were obtained by fitting the Michaelis–Menten model to the depletion curves for each treatment. These parameters are therefore model-derived estimates rather than directly measured variables, and the initial solution concentrations could not be made identical in every run. Given these methodological constraints, conventional ANOVA on the fitted parameters would be of limited meaning. We therefore interpret the observed trends with caution and avoid overstatement of statistical significance.

2.5 Michaelis–Menten equation

The kinetics of potassium and phosphate uptake by the test seedlings were evaluated with a linear fit using the Michaelis–Menten equation:

$$I = \frac{I_{\text{max}} \cdot C}{K_m + C} \tag{2}$$

where C is the ion concentration, I is the uptake rate at concentration C, I_{max} is the maximum uptake rate, and K_m is the half-saturation constant [24]. The minimum critical concentration for ion absorption (C_{min}) was also calculated, when the I was equal to 0.

3 Results

3.1 Potassium Uptake

The variations in I_{max} and K_m during HVEF-induced potassium uptake are shown in Figure 2. When the electric field intensity increased to 1 kV/cm, I_{max} increased remarkably. When the intensity increased from 1 to 2 kV/cm, I_{max} decreased substantially. Afterwards, the uptake rate showed a sharp increase as the intensity kept on increasing between 2 and 3 kV/cm. In contrast, K_m and C_{min} both exhibited opposite trends with turning points at 1.0 and 2.0 kV/cm (Figure 2). At 3.0 kV/cm, K_m and C_{min} reached minimum values 0.57 and 0.07 mmol/L, respectively.

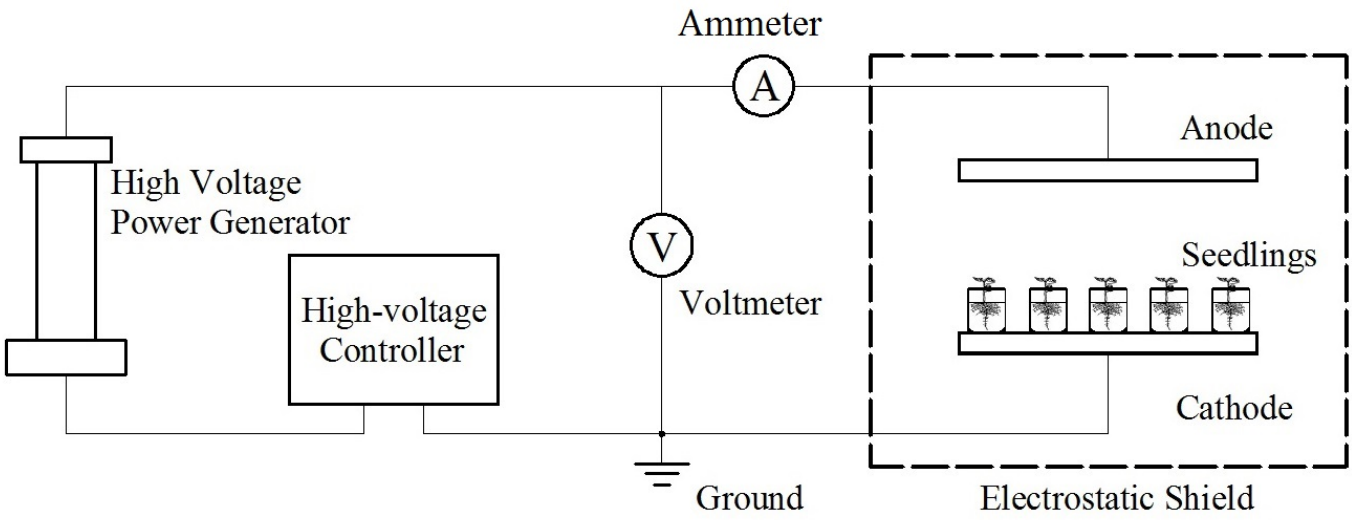

Figure 1. Schematic diagram of the experimental HVEF system. HVEF treatments were performed using a laboratory-scale high electric field apparatus with a maximum output of 100 kV. This apparatus included a BGG100KV/2MA power generator, two rectangular 40 cm×60 cm stainless steel plates used as electrodes, a high-voltage controller, a voltmeter, an ammeter , and an electrostatic shield.

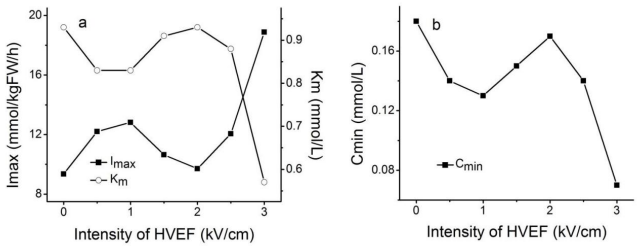

Figure 2. HVEF effects on $I_{\max}$, K_m, and $C_{\min}$ for potassium uptake by cucumber seedlings. *C. sativus* L. seedlings were exposed to electrostatic fields for 7 h at 25 ± 1 °C under a relative humidity of 60%–70% and a photon flux density of 200 μmol/m² s. The control sample was not subjected to high electrostatic fields.

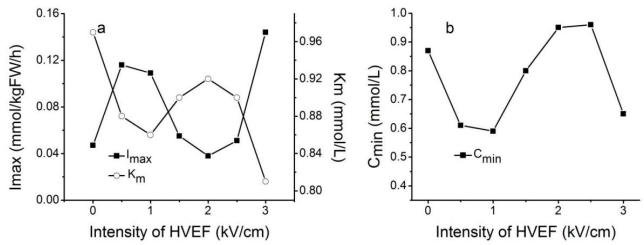

Figure 3. HVEF effects on the kinetics of phosphate uptake. (a) $I_{\max}$ and K_m (b) $C_{\min}$. *C. sativus* L. seedlings were exposed to the field for 7 h at 25 ± 1 °C under a relative humidity of 60%–70% and a photon flux density of 200 μmol/m² s. The control sample was not subjected to high electrostatic fields.

3.2 Phosphate Uptake

Compared with the control sample, an electric field intensity of 0.5 kV/cm caused the phosphate uptake to increase to a maximum value (Figure 3). $I_{\max}$ decreased from this maximum with increasing HVEF intensity for phosphate to reach a minimum at 2 kV/cm. The phosphate uptake rate sharply increased when the intensity of electric field increased from 2 to 3 kV/cm. The variations in K_m and $C_{\min}$ during phosphate uptake were similar as for potassium uptake (Figure 3).

4 Discussion

4.1 Cell Model

As widely acknowledged, the plasma membrane of a plant cell can be modified by an applied transmembrane electric potential [25]. Consequently, the permeability of the membrane can change under an HVEF, especially when the field intensity exceeds a specific threshold [26, 27]. In addition, the cell radius is much larger than the membrane thickness, and the membrane conductance is small compared with that of the internal and external media [28, 29]. Therefore, the effect of HVEF on ion uptake can be qualitatively explained by introducing a simple spherical cell model, in which the starved cell is considered as a uniform conducting sphere surrounded by a thin insulating membrane (Figure 4) [11].

In this model, the electrical conductivity of the extracellular medium, cytoplasm, and membrane are denoted by λ_0, λ_i, and λ_m, respectively. For most healthy cells, the conductivity of the external and

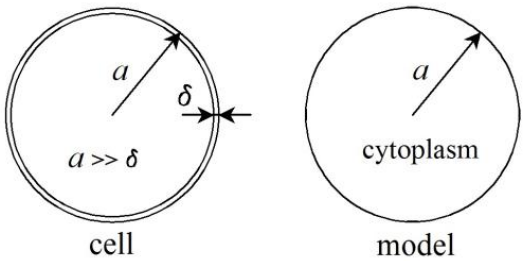

Figure 4. Schematic diagram of cell model. The radius of cell (a) is much larger than the membrane thickness (δ). The model consists of uniform, spherical shells enclosing conductive cytoplasm that could induce a calculable spatial alteration of membrane potential.

internal media are similar and much larger than the effective membrane conductivity:

$$\lambda_0 \sim \lambda_i \gg \lambda_m \left(\frac{\delta}{a}\right) \tag{3}$$

where δ is membrane thickness, a is cell radius.

Under these conditions, the field-induced change in transmembrane potential for a spherical cell exposed to a uniform electric field of strength E can be written as the sum of a direct electric-field term and a surface-charge term [30]:

$$\Delta V_m = \Delta V_{m\text{-direct}} + \Delta V_{m\text{-surface}} \tag{4}$$

The direct term arises from the action of the external field on the cell as a dielectric particle, and is given by the classical Poisson solution:

$$\Delta V_{m\text{-direct}} = \frac{3}{2} E a f \cos\theta \tag{5}$$

where θ is the angle between the radius to the point of observation and the direction of the applied field, f is a dimensionless factor that accounts for the conductivity of the extracellular medium, cytoplasm, and membrane.

$$f = \frac{2\lambda_0\lambda_i}{(2\lambda_0 + \lambda_m)(2\lambda_m + \lambda_i) + \left(\frac{a}{\delta}\right)\lambda_m(2\lambda_0 + \lambda_i)} \tag{6}$$

For most healthy cells, $f \approx 1$ [24–26].

In the present work, $\theta = 0°$ is defined at the upper pole (facing the direction of the field, i.e. toward the positive electrode), and $\theta = 180°$ at the lower pole (opposite to the field direction). This expression predicts that the upper pole ($\theta = 0°$) becomes more positive (depolarized), whereas the lower pole ($\theta = 180°$) becomes more negative (hyperpolarized), while the equatorial region ($\theta \approx 90°$) is only weakly affected.

The surface-charge term arises from electrophoretic redistribution of electromobile charges located at the outer cell surface. Based on Gouy–Chapman theory, the surface potential (ψ) associated with these charges is related to the surface charge density (σ) by [30, 31]:

$$\psi = \left(\frac{2RT}{F}\right) \sinh^{-1}\left(\frac{\sigma}{A}\right) \tag{7}$$

where R is the gas constant, T is the absolute temperature, F is Faraday's constant, and A is a parameter that depends on the ionic strength and dielectric constant of the bathing solution. Combining this relationship with the description of field-driven surface charge redistribution, expression for the surface-charge contribution to ΔV_m is given by [30]:

$$\Delta V_{m\text{-surface}} = \psi_0 - \left(\frac{2RT}{F}\right) \sinh^{-1}\Big\{\sigma_0\big[(1-\nu) + \nu\beta \operatorname{csch}\beta e^{-\beta\cos\theta}\big]/A\Big\} \tag{8}$$

where ψ_0 and σ_0 are the surface potential and surface charge density, respectively, in the absence of an applied field. ν is the mobile fraction of the surface component, β is a dimensionless parameter proportional to the product of field strength, cell radius and the ratio of electrophoretic mobility to diffusion coefficient (m/D), and $\operatorname{csch}\beta = 1/\sinh\beta$ is the hyperbolic cosecant. A is the same parameter as above and depends on the ionic strength and dielectric constant of the medium [28–31].

The actual membrane potential is then:

$$V_m = V_0 + \Delta V_m \tag{9}$$

where V_0 is the resting membrane potential in the absence of HVEF. Although the full analytical form of $\Delta V_{m\text{-surface}}$ is complex, the combined model consistently predicts that the membrane potential becomes more positive in one hemisphere and more negative in the opposite hemisphere under a uniform external field. This angular dependence of V_m (from $\theta = 0°$ to $\theta = 180°$) is the key feature used here to explain the opening and closing of voltage-gated ion channels under HVEF.

For convenience, we define the membrane potentials at the upper and lower poles of the cell as V_t and V_b, respectively. With the above convention, the membrane potentials at the two poles can be written as:

$$V_t = V_0 + \frac{3}{2}Eaf + \psi_0 - \left(\frac{2RT}{F}\right)\sinh^{-1}\left\{\sigma_0\left[(1-\nu)+\nu\beta\,\mathrm{csch}\,\beta e^{-\beta}\right]/A\right\} \tag{10}$$

$$V_b = V_0 - \frac{3}{2}Eaf + \psi_0 - \left(\frac{2RT}{F}\right)\sinh^{-1}\left\{\sigma_0\left[(1-\nu)+\nu\beta\,\mathrm{csch}\,\beta e^{\beta}\right]/A\right\} \tag{11}$$

4.2 Application of model

The analysis in 4.1 shows that a uniform HVEF induces an angularly dependent change in membrane potential, with the upper pole becoming depolarized and the lower pole hyperpolarized as the field strength increases. This asymmetric polarization provides a simple physical basis for the preferential opening of inward-rectifying channels (I_{in}) on the hyperpolarized side and outward-rectifying channels (I_{out}) on the depolarized side.

Two types of ion channels showing characteristic voltage dependence have been identified. Inward-rectifying ion channels open under hyperpolarization conditions and facilitate ion uptake. Outward-rectifying ion channels open under depolarization conditions and enable an outward ion current at relatively positive voltages [9]. Because the plants had been treated with a starvation medium, the resting membrane potential V_0 was below the activation threshold A_i for inward-rectifying channels and had approximately the same value on the upper and lower hemispheres of the cell.

Changes in cell membrane permeability involving membrane hyperpolarization and depolarization occurred in three stages as the applied field increased.

In stage I, the direct field term causes a moderate polarization of the cell membrane. When the applied HVEF intensity increases to E_1 (Figure 5(b)), the absolute value of the bottom membrane potential (V_{b1}) approaches the critical voltage for inward-rectifying ion channels (A_i), so these channels adopt an "open" conformational state. In contrast, the top membrane potential (V_{t1}) does not reach the critical voltage for outward-rectifying ion channels (A_o), and therefore I_{out} channels remain closed. Qualitatively, this can be written as:

$$V_{t1} < A_o \tag{12}$$

$$|V_{b1}| \approx A_i \tag{13}$$

For field strengths in the range $E_1 < E < E_2$ (Figure 5(c)), the area of membrane supporting outward current (I_{out}) is essentially zero, whereas the area supporting inward current (I_{in}) increases with HVEF intensity because $|V_{b1}|$ increases with E. This results in a net absorbing area on the lower hemisphere. In this range, ion absorption increases with the applied field until nearly the entire lower hemisphere is in the absorbing state.

In stage II ($E \approx E_2$ in Figure 5(d), $E > E_2$ in Figure 5(e)), the entire lower hemisphere of the cell remains in the absorbing state (I_{in} fully active), and the I_{in} area changes little with further increases in field strength. In this stage, the top membrane potential (V_{t2}) now exceeds the critical voltage A_o for outward-rectifying ion channels, indicating that I_{out} channels adopt an "open" conformational state:

$$V_{t2} > A_o \tag{14}$$

In this stage, V_{t2} increases with the applied field, which leads to an increase in the area supporting I_{out}. The difference between the I_{in} and I_{out} areas decrease as the intensity increases, until almost the whole upper hemisphere of the cell is in the outward-rectifying state (stage II, Figure 5(e)). This implies that further increases in HVEF will reduce net ion absorption in this stage.

In stage III, when the field strength reaches E_3 (Figure 5(f)), the membrane potential at the depolarized upper pole (V_{t3}) exceeds a critical value (V_c) for voltage-gating effects and electroporation occurs, leading to a sharp increase in cell membrane permeability [32–39]. Using the expression for $\Delta V_m(\theta)$ (Eqs. 7, 9 and 11), this condition can be summarized as:

$$|\Delta V_m|_{\theta=0^\circ} \geq V_c \tag{15}$$

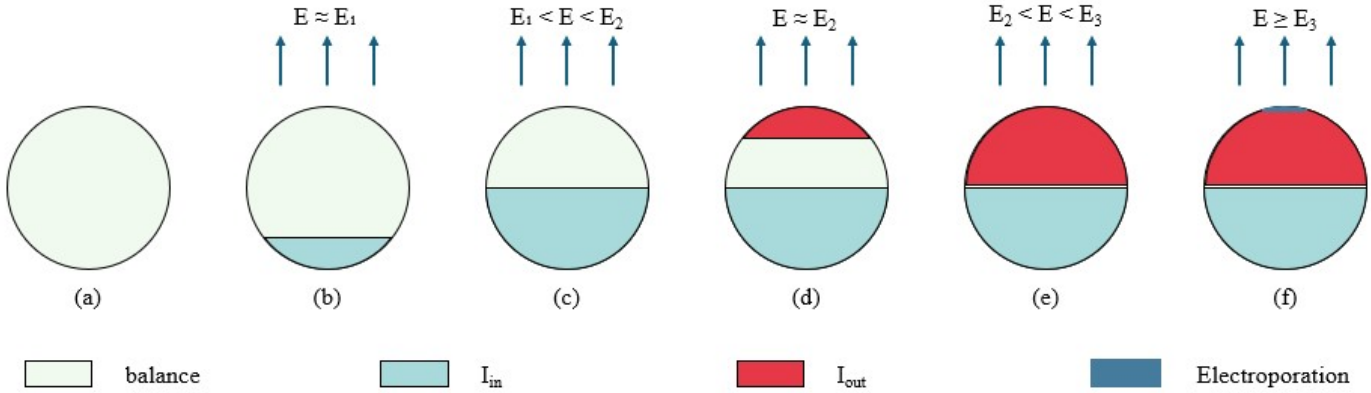

Figure 5. Schematic diagram showing the changes in membrane potential and ion absorption induced by an electric field. The different colors in the figure indicate different membrane potential (V_m) which conduct different kinds of ion current (I_{in}), (balance) and (I_{out}).

At this stage, the formation of transient pores in the membrane greatly enhances transmembrane transport. Although not fully understood, pore formation may generate openings through which even large molecules can enter the cell membrane [35–43], dramatically enhancing ion and solute uptake.

To further illustrate how HVEF modulates the spatial distribution of membrane potential, the dependence of V_m on the angular position θ was calculated for a spherical cell under different field strengths (Figure 6). In the absence of an applied field, V_m is uniform and equal to the resting potential V_0. As E increases, the direct term $\frac{3}{2}Eaf\cos\theta$, together with the surface-charge contribution, generates an approximately cosine-shaped variation in V_m: the upper pole ($\theta = 0°$) becomes progressively depolarized, while the lower pole ($\theta = 180°$) becomes progressively hyperpolarized, and the equatorial region ($\theta \approx 90°$) remains close to V_0. At higher field strengths, the magnitude of this angular modulation increases, and V_m at the upper pole approaches the critical potential V_c for electroporation, in agreement with the three-stage scenario described above.

Taken together, the three stages described above (stage I: mainly I_{in}; stage II: competition between I_{in} and I_{out}; stage III: electroporation-enhanced transport) provide a coherent qualitative framework to interpret the non-monotonic changes in I_{max}, K_m and C_{min} for both K^+ and $H_2PO_4^-$ uptake under HVEF. At lower fields (E around E_1), HVEF primarily enhances the effective membrane area for inward ion flux. At intermediate fields (E between E_1 and E_2), it promotes both inward and outward fluxes and may partially inhibit net uptake. At the highest fields ($E \geq E_3$), electroporation superimposes a non-specific increase in membrane permeability, which explains the sharp increase in I_{max} despite the concurrent expansion of outward-rectifying regions.

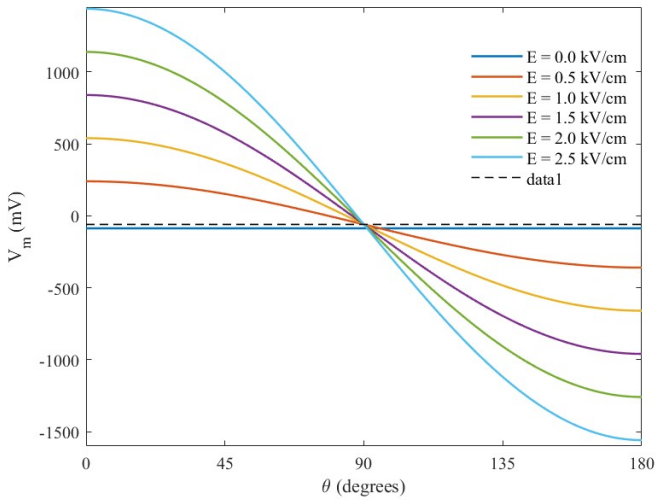

Figure 6. Plasma membrane potential V_m of an 8-μm diameter spherical cell as a function of angle θ for an initial membrane potential V_0 of 60 mV. The value of the mobile fraction ν was 0.9. Electron microscopy provided a mean a value of approximately 4.0 μm [12, 41, 44]. The cell was exposed to a series of uniform electric fields.

4.3 Prospects and Limitations

HVEF, as an energy-saving physical regulation method, has broad application prospects in agricultural production. By adjusting the intensity of HVEF, it may be possible to specifically regulate the uptake of potassium and phosphate by plants, which is of great significance for improving fertilizer use efficiency and reducing environmental pollution. In combination

with optimized fertilization strategies, targeted HVEF treatments could thus contribute to more sustainable nutrient management in intensive cropping systems.

However, several limitations of this study should be acknowledged. First, all experiments were conducted under controlled laboratory conditions using nutrient solutions and starved seedlings. The extent to which HVEF can influence nutrient uptake in soil-grown plants under field conditions remains uncertain and requires further verification. Second, the theoretical model developed here is tailored to K^+ and $H_2PO_4^-$ uptake and relies on a simplified spherical cell geometry and steady-state assumptions. Whether the same mechanisms apply to other nutrient ions, ion pairs or more complex root architectures needs to be examined.

Third, the kinetic parameters ($I_{\max}$, K_m and $C_{\min}$) were obtained using a solution-depletion technique and model fitting. Each uptake experiment consisted of a full depletion time course rather than a single end-point measurement, so the kinetic parameters are model-derived estimates rather than directly measured variables, and conventional statistical tests are not straightforward to apply. We therefore interpret the observed trends with caution and avoid overstatement of statistical significance. Finally, the long-term effects of repeated or continuous HVEF exposure on plant growth, development and metabolic pathways remain largely unknown. Future work should address whether chronic HVEF treatments induce physiological adaptation or stress responses that might alter nutrient uptake kinetics over longer time scales and under realistic field conditions.

5 Conclusion

In this study, the kinetics of potassium and phosphorus uptake by *C. sativus* L. seedlings under HVEF conditions were investigated using the Michaelis-Menten equation. The applied HVEF intensity substantially altered the rate and affinity of potassium and phosphate absorption. An intensity of 1.0 kV/cm was found to substantially enhance the absorption by the cucumber seedlings without causing electroporation of the cells. A cell membrane potential model was constructed to elucidate the effect of HVEF on this absorption process. However, it is unclear whether this mechanism applies to the uptake of other ion species, necessitating further investigation. Given that the biological applications of HVEF require minimal energy, they hold potential for further exploration to either enhance or inhibit the uptake of specific ions by plants.

Future work should evaluate the effects of HVEF on nutrient uptake under field conditions and in soil-grown plants, and assess whether the proposed mechanism applies to other essential ions. In addition, the long-term impacts of repeated HVEF exposure on plant growth, development and stress responses remain to be elucidated. Such studies will help determine how HVEF can be integrated into sustainable fertilization and crop management strategies.

Data Availability Statement

Data will be made available on request.

Funding

This work was supported without any funding.

Conflicts of Interest

The authors declare no conflicts of interest.

AI Use Statement

The authors declare that generative AI was used solely for language translation during the preparation of this manuscript. Specifically, Doubao was used to assist with partial translation from Chinese to English. The authors reviewed and edited all AI-generated content to ensure accuracy, clarity, and consistency with the intended scientific meaning.

Ethical Approval and Consent to Participate

Not applicable.

References

[1] Wu, Y., & Xing, D. (2025). Inaugural editorial for the Journal of Plant Electrobiology. *Journal of Plant Electrobiology, 1*(1), 1–6. [CrossRef]

[2] Murr, L. E. (1963). Plant growth response in a simulated electric field-environment. *Nature, 200*(4905), 490-491. [CrossRef]

[3] Nechitailo, G., & Gordeev, A. (2001). Effect of artificial electric fields on plants grown under microgravity conditions. *Advances in Space Research, 28*(4), 629–631. [CrossRef]

[4] Moon, J. D., & Chung, H. S. (2000). Acceleration of germination of tomato seed by applying AC electric and magnetic fields. *Journal of Electrostatics, 48*(2), 103–114. [CrossRef]

[5] Sidaway, G. H. (1966). Influence of electrostatic fields on seed germination. *Nature, 211*(5046), 303-303. [CrossRef]

[6] Sidaway, G. H., & Asprey, G. F. (1968). Influence of electrostatic fields on plant respiration. *International Journal of Biometeorology, 12*(4), 321-329. [CrossRef]

[7] Li, M. Q., Wu, Y. Y., Zhang, M. M., & Zhu, J. Y. (2018). High-voltage electrostatic fields increase nitrogen uptake and improve growth of tomato seedlings. *Canadian Journal of Plant Science, 98*(1), 93-106. [CrossRef]

[8] Wu, Y., Zhu, J., Li, Y., & Li, M. (2016). Effect of high-voltage electrostatic field on inorganic nitrogen uptake by cucumber plants. *Transactions of the ASABE, 59*(1), 25-29. [CrossRef]

[9] Maathuis, F. J., Ichida, A. M., Sanders, D., & Schroeder, J. I. (1997). Roles of higher plant K+ channels. *Plant Physiology, 114*(4), 1141. [CrossRef]

[10] Schachtman, D. P., Reid, R. J., & Ayling, S. M. (1998). Phosphorus uptake by plants: from soil to cell. *Plant physiology, 116*(2), 447-453. [CrossRef]

[11] Gross, D., Loew, L. M., & Webb, W. W. (1986). Optical imaging of cell membrane potential changes induced by applied electric fields. *Biophysical journal, 50*(2), 339-348. [CrossRef]

[12] Zhu, J. K. (2003). Regulation of ion homeostasis under salt stress. *Current opinion in plant biology, 6*(5), 441-445. [CrossRef]

[13] Etherton, B., & Higinbotham, N. (1960). Transmembrane potential measurements of cells of higher plants as related to salt uptake. *Science, 131*(3398), 409-410. [CrossRef]

[14] Gassmann, W., & Schroeder, J. I. (1994). Inward-rectifying K+ channels in root hairs of wheat (a mechanism for aluminum-sensitive low-affinity K+ uptake and membrane potential control). *Plant Physiology, 105*(4), 1399-1408. [CrossRef]

[15] Ullrich, W. R., & Novacky, A. (1981). Nitrate-dependent membrane potential changes and their induction in Lemna gibba G 1. *Plant Science Letters, 22*(3), 211-217. [CrossRef]

[16] Siddiqi, M. Y., Glass, A. D. M., Ruth, T. J., & Rufty, T. W. (1990). Studies of the uptake of nitrate in barley I. Kinetics of $^{13}NO_3^-$ influx. *Plant Physiology, 93*(4), 1426–1432. [CrossRef]

[17] McClure, P. R., Kochian, L. V., Spanswick, R. M., & Shaff, J. E. (1990). Evidence for cotransport of nitrate and protons in maize roots: I. Effects of nitrate on the membrane potential. *Plant Physiology, 93*(1), 281-289. [CrossRef]

[18] McClure, P. R., Kochian, L. V., Spanswick, R. M., & Shaff, J. E. (1990). Evidence for cotransport of nitrate and protons in maize roots II. Measurement of NO_3^- and H+ fluxes with ion-selective microelectrodes. *Plant Physiology, 93*(1), 290–294. [CrossRef]

[19] Iqbal, B., Zhou, H., Raheem, A., Inamullah, Zheng, T., Khan, A. R., ... & Du, D. (2025). The Impact of Land Use Changes and Agricultural Practices on Phosphorus Cycling: A Review. *Land Degradation & Development*. [CrossRef]

[20] Iqbal, B., Khan, I., Javed, Q., Alabbosh, K. F., Inamullah, I., Zhou, Z., & Rehman, A. (2023). The high phosphorus incorporation promotes the soil enzymatic activity, nutritional status, and biomass of the crop. *Polish Journal of Environmental Studies, 32*(3), 2125-2139. [CrossRef]

[21] Fu, S., Iqbal, B., Alahmadi, T. A., Ansari, M. J., Jalal, A., Nazir, M. J., Li, G., & Du, D. (2025). Ammonium nitrate enhances salinity stress tolerance by inducing physiological and phytohormonal regulation changes in Vigna radiata L. *Global Nest Journal, 27*(6), 07514.

[22] Khan, A. A., Alabbosh, K. F., Kashif, Iqbal, B., Manan, S., Alhoqail, W. A., ... & Wang, Y. F. (2025). Ion Homeostasis, Osmotic Adjustment, and ROS Detoxification Underlie Pea Salinity Tolerance Induced by Pseudomonas putida RT12. *Microbiology Research, 16*(11), 227. [CrossRef]

[23] Drew, M. C., Saker, L. R., Barber, S. A., & Jenkins, W. (1984). Changes in the kinetics of phosphate and potassium absorption in nutrient-deficient barley roots measured by a solution-depletion technique. *Planta, 160*(6), 490–499. [CrossRef]

[24] Down, J. E., & Riggs, D. S. (1965). A comparison of estimates of Michaelis-Menten kinetic constants from various linear transformations. *Journal of Biological Chemistry, 240*(2), 863–869.

[25] Cole, K. S. (1972). *Membranes, ions and impulses: a chapter of classical biophysics* (Vol. 1). Univ of California Press.

[26] Hille, B. (1978). Ionic channels in excitable membranes. Current problems and biophysical approaches. *Biophysical journal, 22*(2), 283-294. [CrossRef]

[27] Doyle, D. A., Cabral, J. M., Pfuetzner, R. A., Kuo, A., Gulbis, J. M., Cohen, S. L., ... & MacKinnon, R. (1998). The structure of the potassium channel: molecular basis of K+ conduction and selectivity. *science, 280*(5360), 69-77. [CrossRef]

[28] Jaffe, L. F. (1977). Electrophoresis along cell membranes. *Nature, 265*(5595), 600-602. [CrossRef]

[29] Poo, M. M. (1981). In situ electrophoresis of membrane components. *Annual Review of Biophysics and Bioengineering, 10*, 245–276. [CrossRef]

[30] Gross, D. A. V. I. D. (1988). Electromobile surface charge alters membrane potential changes induced by applied electric fields. *Biophysical journal, 54*(5), 879-884. [CrossRef]

[31] Teissie, J., & Rols, M. P. (1993). An experimental evaluation of the critical potential difference inducing cell membrane electropermeabilization. *Biophysical journal, 65*(1), 409-413. [CrossRef]

[32] Lojewska, Z., Farkas, D. L., Ehrenberg, B., & Loew, L. M. (1989). Analysis of the effect of medium and membrane conductance on the amplitude and kinetics of membrane potentials induced by externally applied electric fields. *Biophysical journal, 56*(1), 121-128. [CrossRef]

[33] Tekle, E., Astumian, R. D., & Chock, P. B. (1990). Electro-permeabilization of cell membranes: effect of the resting membrane potential. *Biochemical and biophysical research communications, 172*(1), 282-287. [CrossRef]

[34] Hibino, M., Shigemori, M., Itoh, H., Nagayama, K., & Kinosita, K. (1991). Membrane conductance of an electroporated cell analyzed by submicrosecond imaging of transmembrane potential. *Biophysical journal, 59*(1), 209-220. [CrossRef]

[35] Teissié, J., Eynard, N., Gabriel, B., & Rols, M. P. (1999). Electropermeabilization of cell membranes. *Advanced drug delivery reviews, 35*(1), 3-19. [CrossRef]

[36] Neumann, E., Sowers, A. E., & Jordan, C. A. (1989). *Electroporation and electrofusion in cell biology* (pp. 59–164). Springer. [CrossRef]

[37] Zimmermann, U., & Neil, G. A. (1996). *Electromanipulation of cells* (pp. 1–106). CRC Press.

[38] Weaver, J. C. (2002). Electroporation of cells and tissues. *IEEE transactions on plasma science, 28*(1), 24-33. [CrossRef]

[39] Schoenbach, K. H., Joshi, R. P., Kolb, J. F., Chen, N., Stacey, M., Blackmore, P. F., ... & Beebe, S. J. (2004). Ultrashort electrical pulses open a new gateway into biological cells. *Proceedings of the IEEE, 92*(7), 1122-1137. [CrossRef]

[40] Chapel, M., Teissié, J., & Alibert, G. (1984). Electrofusion of spermine-treated plant protoplasts. *FEBS Letters, 173*(2), 331–336. [CrossRef]

[41] Puite, K. J. (1992). Progress in plant protoplast research. *Physiologia Plantarum, 85*(2), 403–410. [CrossRef]

[42] Glaser, R. W., Leikin, S. L., Chernomordik, L. V., Pastushenko, V. F., & Sokirko, A. I. (1988). Reversible electrical breakdown of lipid bilayers: formation and evolution of pores. *Biochimica et Biophysica Acta (BBA)-Biomembranes, 940*(2), 275-287. [CrossRef]

[43] Gowrishankar, T. R., Chen, W., & Lee, R. C. (1998). Non-Linear Microscale Alterations in Membrane Transport by Electropermeabilization a. *Annals of the New York Academy of Sciences, 858*(1), 205-216. [CrossRef]

[44] Maathuis, F. J., & Sanders, D. (1996). Mechanisms of potassium absorption by higher plant roots. *Physiologia Plantarum, 96*(1), 158-168. [CrossRef]

Jianyun Zhu obtained his Master's degree in Agricultural Mechanization Engineering from Jiangsu University, China, in 2014, and his Ph.D. degree in Ship Engineering from Shanghai Jiao Tong University, China, in 2021. (Email: Dr.JYZhu@outlook.com)

Meiqing Li holds a Ph.D. in plant nutrition science from Shandong Agricultural University. Her research focuses on plant nutrition, plant stress physiology, and nutrition detection. She has successfully applied electrical impedance spectroscopy(EIS) techniques to investigate plant nutrient stress, and explored the ameliorative effects of exogenous hormone application on quinoa under stress conditions. (Email: lmqljy@163.com)